Atmospheric Pressure Plasma Acoustic Moment Analysis

Victor J. Law

Dublin City University
National Centre for Plasma Science and Technology
Collins Avenue, Glasnevin, Dublin 9, Dublin, Ireland

Feidhlim T. O'Neill
Denis P. Dowling

School of Electrical, Electronic, and Mechanical Engineering
University College Dublin
Belfield, Dublin 4, Ireland

Low-order moment around the mean (mean, standard deviation, and skewness) analysis of the time evolution of specific acoustic intensities of an air atmospheric pressure plasma jet is performed as a function of nozzle-to-surface gap (0.5 to 7 cm), drive frequency (19, 22, and 25 kHz), and air flow rate (35.7 to 76.6 l/m). The probability distribution of each time-series dataset exhibits deterministic correlations with contrasting entropy process regions in the afterglow (blown arc process (gap = 0.5 cm and 1740 ±100 K); and gap = 1 to 7 cm and 300 to 400 K)). The results indicate that the heated air is channeled along the surface and has a preferred backscatter angular. In addition, the blown arc process exhibits a skewness of +0.055 and the afterglow has skewness values from –0.05 to –0.4. These results illustrate how acoustic information can be used to differentiate plasma-surface entropy states.

1. Introduction

Complex systems that contain electro- and bio-mechanical elements emit characteristic acoustic noise that can be recognized by the human ear. In an attempt to automate this human sensory behavior, noninvasive acoustic metrology has attracted much interest in the semiconductor manufacturing industry [1], nuclear power generation [2], plasma welding [3], environment monitoring [4, 5], and the food health sector [6]. Within this body of work, multivariate analysis tools such as principal component analysis and low-order moment analysis (mean, standard deviation, skewness, and kurtosis) have been used to separate the deterministic component from the stochastic (background) noise. Recently, real-time noninvasive acoustic metrology, at a specific frequency and over a given frequency range, has been applied to atmospheric pressure plasma (APP) to measure electrical performance [7, 8], identify the APP jet nozzle [9, 10], and generate an acoustic image of the treatment surface [10]. The ability to

https://doi.org/10.25088/ComplexSystems.20.2.181

map the treated surface and estimate the temperature of the process has immense technological importance when processing temperature-sensitive materials such as polymers and biological materials. The impact of this technology offers enhanced quality of care at reduced cost and will be of immense societal and commercial value.

This paper examines the specific acoustic intensity at a fixed distance of 9 cm from an atmospheric pressure plasma jet (APPJ) as it is positioned over typical ceramic and steel surfaces that are employed within the automobile, aerospace, and medical device manufacturing sectors. The analysis approach used in this paper is based on the assumption that an acoustic point-source (of finite volume) generates a time-varying signal that has a Gaussian probability distribution, and that the introduction of a deterministic component (i.e., elongation of acoustic source volume) will alter the time-varying signal probability distribution. Linear statistical analysis of the first three orders of moments around the mean (mean, standard deviation, and skewness) are used to construct Cartesian low-order shape-space diagrams that delineate the known temperature regions between the plasma [9, 10] and the treated surface. The use of acoustic low-order moments may be considered analogous to the term "timbre," which distinguishes source(s) of sound production of a musical tone. This approach has the additional advantage of using all the sampled time sequence data points, as compared to using a reduced dataset of extreme minimum and maximum time series values of the original dataset as proposed by Kugiumtzis [11] and used by Charakopoulos et al. [12] when monitoring human brain activity and turbulence in jet systems. The disadvantage of using the minimum and maximum approach is that up to 75% of the original dataset may be lost [12] which may have an impact on the discrimination potency. However, it must be stated that the third order of moment around the mean (skewness) needs careful interpretation because a zero skewness does not imply that the mean is equal to the median, as in the case of discrete distributions that are multimodal or have a significant kurtosis component. Given this corollary, the skewness criteria must have additional supportive evidence when used as a metrology tool.

2. Atmospheric Pressure Plasma Jet and Acoustic Hardware

The APPJ used in this work is the pilot scale PlasmaTreat Open-Air system manufactured by PlasmaTreat GmbH. The working gas is compressed air (1000 to 3000 mbar and 35.6 to 76.6 liters per minute (l/m)). The system is electrically powered using a 19 to 25 kHz high voltage positive uni-polar square-wave pulse-width modulated power supply with an effective duty cycle of 50%. The APPJ is mounted on a computer numerically controlled gantry allowing full XYZ positioning over a treatment surface. When the APPJ is turned on, the sound

https://doi.org/10.25088/ComplexSystems.20.2.181

pressure level increased between 90 and 103 dB at an applied dc pulse voltage of 10 kV and duty cycle of 10 to 100%. For full details of the APPJ, see [8–10, 13, 14].

An omni-directional condenser microphone positioned perpendicular to the APPJ nozzle at a distance of 9 cm acts as both a sound sensor and as a near-field E-probe. The functional duality of the microphone captures the electro-acoustic emission of the APPJ and converts the signals into a convoluted analog voltage, which in turn is passed to a Dell Precision M90 laptop computer that is fitted with a Sigma Tel Audio soundcard. The soundcard digitizes the analog signal for real-time processing using National Instruments LabVIEW software. Figure 1 provides a photograph of a 19 kHz driven air APPJ along with the nitrogen gas rotational temperature as a function of discharge axial regions; these are blown arc and flowing afterglow (near and far regions).

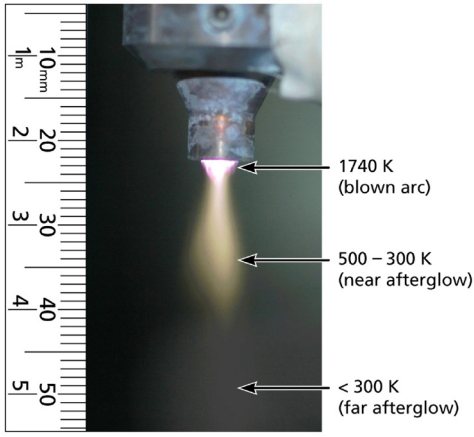

Figure 1. Photograph of the Open-Air APPJ with the N_2 rotational temperature as a function of discharge axial distance.

The LabVIEW (version 8.2) software program samples the acoustic data over a frequency range between 0 to 25 kHz to produce a frequency spectrum with resolution of one data point per Hz. The acoustic frequency spectrum then undergoes conditioning using a Savitzky–Golay (SG) digital filter [15]. The SG filter smooths the spectrum data points by least square minimization with a polynomial function ($m = 1$) within a symmetrical moving window,

$$2k + 1, \tag{1}$$

where k are the ± sampled data points on either side of the interrogated data point. In this work, a k value of 10 Hz preserves the rapid rise and fall times of the electrical component (the power supply drive

https://doi.org/10.25088/ComplexSystems.20.2.181

signal and its harmonics) in the convoluted electro-acoustic signal and thus prevents the digital moving window filter process from over sampling according to the Nyquist–Shannon criteria [16, 17]. This approach differs from the technique of delay embedding to calculate the average mutual information (AMF) [18, 19], which in information theory is analogous to the autocorrelation function. Following the previous work of Law et al. [9, 10], the frequency at which the surface provides a specific acoustic intensity (SAI) response (8 kHz) is interrogated at a sampling rate of 1 data point per 0.5 seconds as a function of both time and space. Figure 2 provides two typical APPJ time-varying SAI traces at a nozzle-to-surface gap distance of 0.5 cm and 7 cm, respectively. The electrical drive frequency is 19 kHz. For clarity only, the time-traces contain $N = 300$ data points with each point corresponding to a 1 second increment in time. Figure 3 depicts the probability distribution histogram for the 0.5 cm and 7 cm datasets, but over an extended time of 200 seconds. The number of bins for each dataset is determined using the $\sqrt{N}$ criteria, where N is the number of data points. Given the two types of data (time-trace and probability distribution histogram) presented, a clear visual differentiation can be seen between the datasets that represent contrasting plasma processing applications. First, consider the two time-traces in Figure 2. Both traces show no sign of periodicity but fluctuate over an amplitude span of approximately 5 dB. Second, their mean SAI values are significantly different (–53.6 dB for the 0.5 cm dataset and –57.8 dB for the 7 cm dataset). The mean acoustic amplitude difference (4.2 dB) is primarily due to acoustic reflection from the surface; this aspect is discussed later. Third, the two histograms have a Gaussian fitted. The curves show that the 0.5 cm dataset presents a near normal probability distribution whereas the 7 cm dataset is weighted (skewed) to lower acoustic amplitudes.

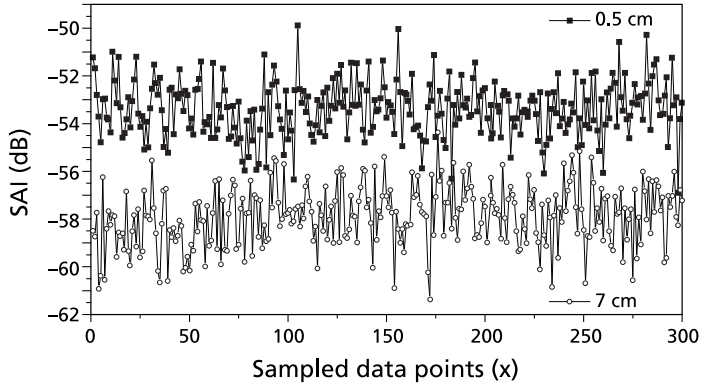

Figure 2. Typical APPJ acoustic emission time-trace (sampling period = 300 seconds). The solid line = 0.5 cm and the dashed line = 7 cm nozzle-to-surface gap distances. The electrical drive frequency is 25 kHz.

https://doi.org/10.25088/ComplexSystems.20.2.181

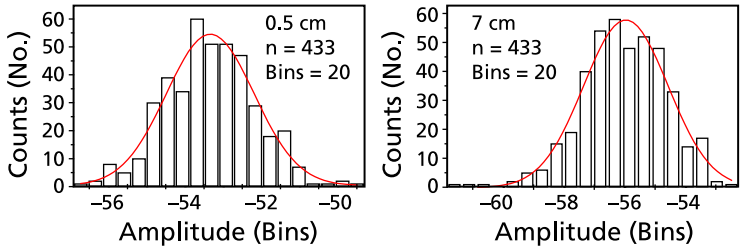

Figure 3. Probability distribution histograms for nozzle-to-surface gap distances of 0.5 cm and 7 cm. Data points = 433 and 20 bins.

To quantify the observed differences within these datasets and others, a metrology method needs to be introduced to describe, compare, and contrast the shapes of the datasets. In addition, the goal of this metrology is to extract useful spatial and temperature process information. The final part of this section sets out the mathematical metrology to achieve this goal.

The metrology used here is based upon low-order moment analysis of time series data of length N, $x(t)$, $t = 1, 2, \ldots N$. This methodology is used to discriminate and define the vertical surface location and process temperature by calculating the first three moments around the acoustic mean intensity. These are: Mean (μ),

$$\mu = \frac{1}{N}\sum_{i=0}^{n-1} x_j; \tag{2}$$

standard deviation (σ),

$$\sigma = \frac{1}{N}\sum_{i=0}^{n-1} (x_j - \mu); \tag{3}$$

and the normalized third order moment ((γ_1), skewness). The value γ_1 is calculated using equations (3) and (5):

$$\gamma_1 = \frac{\mu^3}{\sigma^3}, \tag{4}$$

$$\mu_x^3 = \frac{1}{N}\sum_{i=0}^{n-1} (x_j - \mu)^3. \tag{5}$$

In equation (4), μ^3 is the third moment of the mean, and σ_x^3 is the standard deviation to the power of 3 of the dataset. In equation (5) μ^3 is calculated, where N is the number of elements (433) in the sampled

https://doi.org/10.25088/ComplexSystems.20.2.181

time sequence x. It is important to note that a zero value indicates the distribution is relatively evenly distributed on both sides of the mean; the distribution could be bimodal and have a significant kurtosis component.

3. Shape-Space Analysis

In this work, 40 time-varying SAI measurements are made with each measurement containing 433 sampled values over 216 seconds. The measurements were made as follows: 20 ceramic samples at 25 kHz, 14 ceramic samples at 19 kHz, and six steel samples at 25 kHz. The measurements are further characterized by a fixed nozzle-to-surface gap of 7 to 0.5 cm at either 1 or 0.5 cm step intervals. Under these varying gap distance values, the APPJ discharge temperature region in contact with the surface changes from far afterglow (300 to 290 K) at 7 cm, through the near afterglow at 0.5 cm to between 3 and 4 cm (500 to 300 K), and to the blown arc region (1740 ±100 K) at 0.5 cm. In addition, the microphone incident angle reduces from 38 to 3 degrees.

Figure 4 shows the mean acoustic intensity (μ) for all 40 time-varying SAI measurements as a function of gap distance and microphone incident angle. The acoustic data has two nodes (1 to 3.5 cm and 4 to 7 cm) within a common μ decline as the nozzle-to-surface gap increases. The severance point (4 cm) between these nodes is associated with the visible afterglow from the surface. This phonological feature suggests that cooled ions arriving at the surface have a role in the acoustic noise process as the reflected molecular gas is channeled along the perpendicular surface. A preferred microphone incident angle of 25 to 35 degrees is used. Three further features of note are: first, that the μ values decreases with drive frequency; second, air flow rate has an effect on the acoustic level; and third, the comparative ceramic and steel surface data exhibit little difference in their μ values. However, the use of μ as a process temperature measurement is limited because there are multiple μ values for a given drive frequency and air flow rate as the nozzle-to-surface varies. For example 3, 5, and 6.5 cm have similar values of $\mu \sim -57$ dB.

In addition to this data, it is necessary to know the run-to-run and day-to-day variation in the SAI measurements. To access this information, the measurement instruments were dismantled and rebuilt every few weeks over a two-month period. The total spread in collected data was found to be ±1 dB. This value is an experiment offset only and did not alter the acoustic outcomes. For clarity, this maximum spread in μ is only shown on the first 19 kHz, 35.7 l/m data point. This day-to-day variation is used as the minimum separation to identify any deterministic effect in shape-space.

https://doi.org/10.25088/ComplexSystems.20.2.181

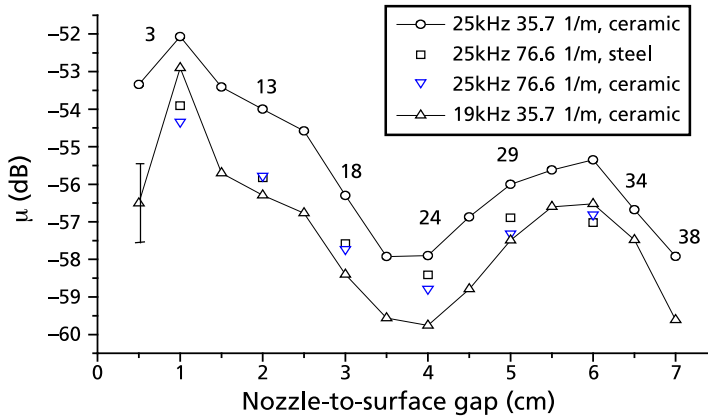

Figure 4. SAI μ plotted against distance and microphone incident angle for steel and ceramic datasets.

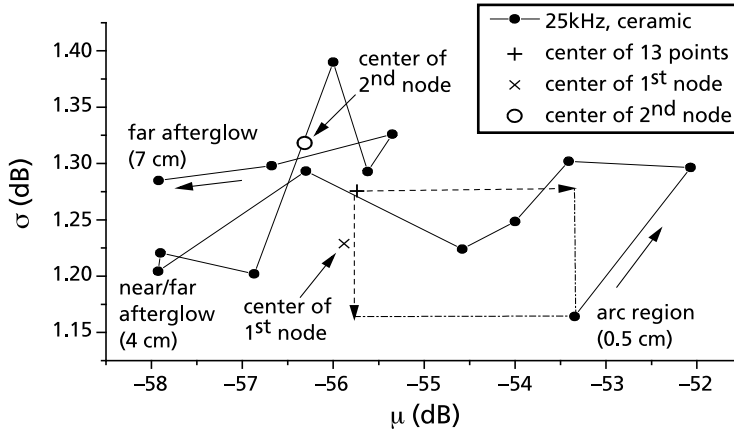

Figure 5. SAI shape-space mapping (μ and σ) for 25 kHz, 35.7 l/m ceramic dataset.

To remove the angular distribution effect the 25 kHz, 35.7 l/m ceramic dataset has been computed for its associated σ values. These values are displayed in Figure 5 within Cartesian shape-space with μ plotted on the abscissa axis and σ plotted on the ordinate axis; also included are the three plasma regions as a function of gap. The shape-space reveals that the 0.5 cm arc process is separated from the remaining 13 data points. Parametric cluster analysis [20] indicates that the arc process is separated by –2.395 μ (dB) to 0.1114 μ (dB) from the averaged center (+) of the remaining 13 data point cluster 9 (see dot-

https://doi.org/10.25088/ComplexSystems.20.2.181

ted box). This separation distance is over twice the measured day-to-day variation as identified in Figure 4. Using this knowledge, it is reasonable to classify the arc process as a separate cluster from the remaining 13 data points. In addition, the 13 data points may be classified as two further subclusters that represent the first (×) and second nodes (◦); where each subcluster ranges between –53 to –58 μ and 1.2 to 1.3 σ; and –55.35 to –57.92 μ and between 1.22 and 1.376 σ, respectively. In the real world these two clusters correlate to the discharge plume disengaging (near afterglow) from the surface and when the plume is free from the surface (far afterglow).

Two additional features of note can be observed in the node data points. First, trajectory analysis reveals that the data point trajectory in the second node is a reversal of the first node's data points. Second, standardization normalization of μ by σ (i.e., μ / σ) for each cluster reveals a bifurcation on the order of 40 to 47, respectively.

Low-order shape-space mapping (μ and σ) has also been performed on the 19 kHz ceramic dataset and is presented in Figure 6. In this case, the arc process is separated from the remaining 13 data points by 3.5 μ (dB). Here again the reversal in trajectory is initiated at the 4 cm point to produce conjugate points having an average of 0.5 μ (dB) separation. Of further note, the standardization of μ (μ / σ) within the remaining 13 data points has an average value of 40. In comparison with the 25 kHz dataset, the day-to-day separation standard (±1 dB) indicates that the arc process is separated even further from the remaining data points and that the remaining points can be classified as a single cluster.

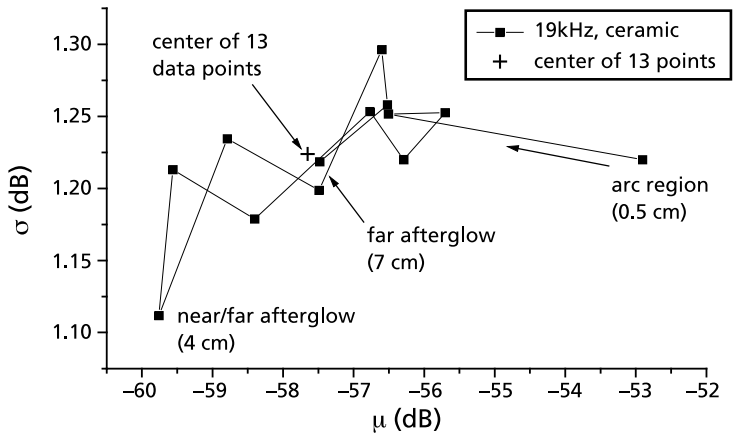

Figure 6. SAI shape-space mapping (μ and σ) for the 19 kHz, 35.7 l/m ceramic dataset.

https://doi.org/10.25088/ComplexSystems.20.2.181

The shape-space mapping has also been extended to μ and γ_1. Results of two-dimensional mapping are not shown here but are described. In this case the arc process has a $\gamma_1 \sim +0.055$, or near-Gaussian distribution, implying that the reduced acoustic source volume resembles a causal pure tone. In addition, as the gap increases, γ_1 becomes negative within the range of -0.5 to -0.42, indicating a causal dependence as the acoustic source volume increases. The use of three low-order moments allows moment analysis to be displayed in three-dimensional Cartesian shape-space. Figure 7 shows this display for the ceramic data using the LabVIEW software, where the three axes are labeled x axis = Mean, y axis = STD, and z axis = Skewness. Using this software, the viewing angle can be rotated in real-time for complete inspection of the shape-space. However, for this paper a fixed orthogonal view is chosen. The display reveals the start (0.5 cm arc) of the data point sequence (coordinates: $\mu = -0.055$, $\sigma = 1.163$, and $\gamma_1 = +0.055$), and the finish point within the cluster (coordinates: $\mu = -57.92$, $\sigma = 1.286$, and $\gamma_1 = -0.140$). The important point here is that the visual separation of the clusters can be maximized by selecting an appropriate viewing angle that is unavailable in a two-dimensional projection.

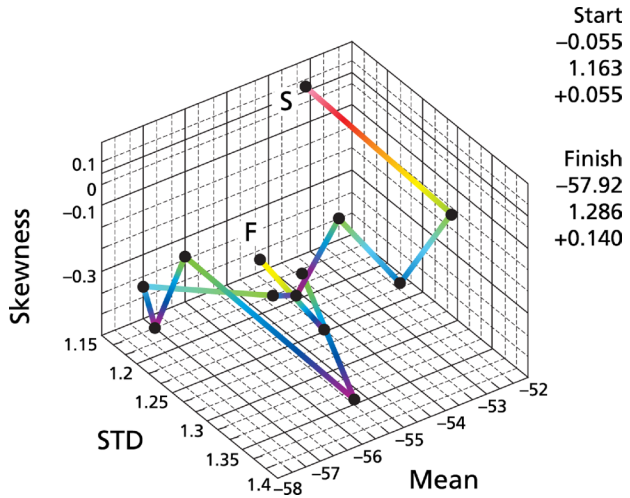

Figure 7. Three-dimensional SAI shape-space representation of low-order values.

https://doi.org/10.25088/ComplexSystems.20.2.181

4. Specific Acoustic Intensity Mapping of Process Parameters

The air flow and drive frequency are known to be important factors that influence plasma processing of polymers [8–10, 19]. Figure 8 shows a triplet of acoustic intensity maps (AIMs) that reveal how μ is defined by drive frequency (19, 22, and 25 kHz) and helium flow at three gap distances (0.5, 3, and 7 cm). The 0.5 cm gap AIM reveals that μ varies by 5 dB across the frequency and only 2 dB across the flow parameter. Within this parameter space a flat acoustic region is produced as both flow and drive frequency are increased. This region is depicted with the letter A. Moving to the 3 cm gap AIM, the magnitude of the iso-acoustic contours decreases and changes in orientation for the same parameter space. This is primarily due to the influence of flow rate at the higher drive frequencies (22 and 25 kHz). At the 7 cm gap distance, a similar AIM is produced to that of the 3 cm position.

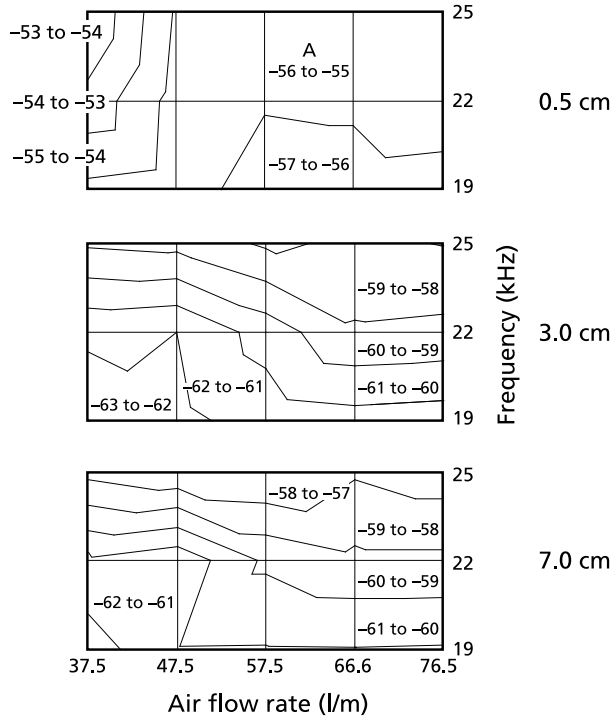

Figure 8. Triplet of specific AIMs depicting the effects of drive frequency and gas flow as a function of gap distance (0.5, 3, and 7 cm) upon mean acoustic intensity.

https://doi.org/10.25088/ComplexSystems.20.2.181

5. Conclusions

This paper has considered the time evolution of the specific acoustic intensity (SAI) at 9 cm from an air atmospheric pressure plasma jet (APPJ) as a function of nozzle-to-surface gap (0.5 to 7 cm). The analysis computes the low-order moments of the acoustic signal (mean, standard deviation, and skewness) and displays the results in Cartesian shape-space followed by parametric cluster analysis. In addition, three-dimensional specific acoustic intensity maps (AIMs) are constructed to follow the APPJ as a function of gas flow, drive frequency, and nozzle-to-surface gap. The analysis reveals a deterministic link within μ, σ, and γ_1 of the APPJ time-varying SAI signal as the gap distance is varied. Under blown arc contact conditions (i.e., reduced volume ~1 cm^3 and maximum temperature) the SAI signal is found to exhibit a pure tone that approaches maximum intensity. As the nozzle-to-surface gap increases, along with the acoustic volume (1 to 20 cm^3), the SAI mean value reduces in a bimodal manner along with an increasingly negative magnitude of skewness. Comparative surface material experiments between steel and ceramic reveal that there is no significant difference in the acoustic measurement. Two-dimensional shape-space (μ, σ) yields data clusters that are correlated to contrasting entropy plasma process regions (blown arc and flowing afterglow), and associated plasma-surface reaction temperatures. The standardization of μ reveals a bifurcation in the 25 kHz, 35.7 l/m dataset as compared to the 17 kHz, 35.7 l/m conditions. The data suggests that there is a causal relationship between the bifurcation and drive frequency. In three-dimensional shape-space, where all low-order moments are used, a further enhancement of the projected shape can be gained. The application of AIMs translates the low-order moments into the real-world parameter-space that can be readily employed in understanding the implications of the acoustic measurement.

In this work, a symmetrical moving window is used to improve the signal-to-noise ratio. However, the use of an asymmetric moving window that mimics a sound attack-sustain-release profile of the original sound signal may increase feature discrimination within the low-order moment analysis. This feature is now being investigated.

Acknowledgments

This work is supported by Science Foundation Ireland 08/SRC/I1411. We would also like to thank Prof. N. Thornhill (Imperial College London, UK) and Dr. N. Jevtic (Bloomsburg University, USA) for helpful discussions regarding this work.

https://doi.org/10.25088/ComplexSystems.20.2.181

References

[1] M. Yasaka, M. Takeshita, and R. Miyagawa, "Detection of Supersonic Waves Emitted from Anomalous Arc Discharge in Plasma Processing Equipment," *Japanese Journal of Applied Physics*, **39**, 2000 pp. L1268–L1288.

[2] T. Biserna, F. Cavallini, S. Taglienti, and V. Tosi, "Results of Acoustic and Temperature Noise Measurements on Sodium Cooled Electrically Heated 7 Rod Bundle," *Progress in Nuclear Energy*, **1**(2–4), 1977 pp. 517–526.

[3] Y. Wang and P. Zhao, "Noncontact Acoustic Analysis Monitoring of Plasma Arc Welding," *International Journal of Pressure Vessels and Piping*, **78**(1), 2001 pp. 43–47. doi:10.1016/S0308-0161(00)00085-5.

[4] I. G. Rees and C. G. Don, "A Portable Microprocessor-Controlled Instrument for Measuring the Moments of an Amplitude Histogram (Acoustic Measurement Application)," *Journal of Physics E: Scientific Instruments*, **16**(9), 1983 pp. 832–835. doi:10.1088/0022-3735/16/9/005.

[5] H. Wu, M. Siegel, and P. Khosla, "Vehicle Sound Signature Recognition by Frequency Vector Principal Component Analysis," *IEEE Transactions on Instrumentation and Measurement*, **48**(5), 1999 pp. 1005–1009. doi:10.1109/19.799662.

[6] A. Zdunek, D. Konopacka, and K. Jesionkowska, "Crispness and Crunchiness Judgment of Apples Based on Contact Acoustic Emission," *Journal of Texture Studies*, **41**(1), 2010 pp. 75–91. doi:10.1111/j.1745-4603.2009.00214.x.

[7] J. Tynan, V. J. Law, P. Ward, A. M. Hynes, J. Cullen, G. Byrne, D. P. Dowling, and S. Daniels, "Comparison of Pilot and Industrial Scale Atmospheric Pressure Glow Discharge Systems Including a Novel Electro-Acoustic Technique for Process Monitoring," *Plasma Sources Science and Technology*, **19**(1), 2010 p. 015015. doi:10.1088/0963-0252/19/1/015015.

[8] D. P. Dowling, F. T. O'Neill, S. J. Langlais, and V. J. Law, "Influence of dc Pulsed Atmospheric Pressure Plasma Jet Processing Conditions on Polymer Activation," *Plasma Processes and Polymers*, **8**(8), 2011 pp. 718–728. doi:10.1002/ppap.201000145.

[9] V. J. Law, F. T. O'Neill, and D. P. Dowling, "Evaluation of the Sensitivity of Electro-Acoustic Measurements for Process Monitoring and Control of an Atmospheric Pressure Plasma Jet System," *Plasma Sources Science and Technology*, **20**(3), 2011 p. 035024. doi:10.1088/0963-0252/20/3/035024.

[10] V. J. Law, D. P. Dowling, J. L. Walsh, F. Iza, N. B. Janson, and M. Kong, "Decoding of Atmospheric Pressure Plasma Emission Signals for Process Control," in *Book of Abstracts from the 4th Chaotic Modeling & Simulation International Conference (CHAOS '11)*, Agios Nikolaos, Crete, Greece (C. H. Skiadas, ed.), 2011 p. 75. http://www.cmsim.org/images/CHAOS2011-Book_of_Abstracts.pdf.

[11] D. Kugiumtzis, A. Papana, A. Tsimpiris, I. Vlachos, and P. G. Larsson, "Time Series Feature Evaluation in Discriminating Preictal EEG States," *Lecture Notes in Computer Science*, **4345**, 2006 pp. 298–310. doi:10.1007/11946465_27.

https://doi.org/10.25088/ComplexSystems.20.2.181

[12] A. Charakopoulos, T. E. Karakasidis, and P. Papanicolaou, "Detection of Jet Axis in a Horizontal Turbulent Jet via Nonlinear Analysis of Minimum/Maximum Temperature Time Series," in *Book of Abstracts from the 4th Chaotic Modeling & Simulation International Conference (CHAOS '11)*, Agios Nikolaos, Crete, Greece (C. H. Skiadas, ed.), 2011 p. 56. http://www.cmsim.org/images/CHAOS2011-Book_of_Abstracts.pdf.

[13] Y. Kubota, R. Ichiki, T. Hara, N. Yamaguchi, and Y. Takemura, "Spectroscopic Analysis of Nitrogen Atmospheric Plasma Jet," *Journal of Plasma and Fusion Research SERIES*, **8**, 2009 pp. 740–73.

[14] J. Pulpytel, V. Kumar, P. Peng, V. Micheli, N. Laidani, and F. Arefi-Khonsari, "Deposition of Organosilicon Coatings by a Non-Equilibrium Atmospheric Pressure Plasma Jet: Design, Analysis and Macroscopic Scaling Law of the Process," *Plasma Processes and Polymers*, **8**(7), 2011 pp. 644–675. doi:10.1002/ppap.201000121.

[15] A. Savitzky and M. J. Golay, "Smoothing and Differentiation of Data by Simplified Least Squares Procedures," *Analytical Chemistry*, **36**(8), 1964 pp. 1627–2639. doi:10.1021/ac60214a047.

[16] H. Nyquist, "Certain Topics in Telegraph Transmission Theory," *Transactions of the American Institute of Electrical Engineers*, **47**(2), 1928 pp. 617–44. doi:10.1109/T-AIEE.1928.5055024 .

[17] C. E. Shannon, "Communication in the Presence of Noise," *Proceedings of the Institute of Radio Engineers*, **37**(1), 1949 pp. 10–21. doi:10.1109/JRPROC.1949.232969 .

[18] J. L. Walsh, F. Iza, N. B. Janson, V. J. Law, and M. G. Kong, "Three Distinct Modes in a Cold Atmospheric Pressure Plasma Jet," *Journal of Physics D: Applied Physics*, **43**(7), 2010 p. 075201. doi:10.1088/0022-3727/43/7/075201.

[19] N. Jevtic, J. S. Schweitzer, and P. Stine, "Optimizing Nonlinear Projective Noise Reduction for the Detection of Planets in Mean-Motion Resonances in Transit Light Curves," in *Chaos Theory: Modeling, Simulation and Applications* (C. H. Skiadas, I. Dimotikalis, and C. Skiadas, eds.), Singapore: World Scientific Publishing, 2010 pp. 191–199. doi:10.1142/9789814350341_0022.

[20] V. J. Law, C. E. Nwankire, D. P. Dowling, and S. Daniels, "Acoustic Emission within an Atmospheric Helium Discharge Jet," in *Chaos in Theory: Modeling, Simulation and Applications* (C. H. Skiadas, I. Dimotikalis, and C. Skiadas, eds.), Singapore: World Scientific Publishing, 2010 pp. 255–264. doi:10.1142/9789814350341_0030.

https://doi.org/10.25088/ComplexSystems.20.2.181